

Adaptive Local Neighborhood-based Neural Networks for MR Image Reconstruction from Undersampled Data

Shijun Liang, *Student Member, IEEE*, Anish Lahiri, *Member, IEEE*,
Saiprasad Ravishankar, *Senior Member, IEEE*

Abstract—Recent medical image reconstruction techniques focus on generating high-quality medical images suitable for clinical use at the lowest possible cost and with the fewest possible adverse effects on patients. Recent works have shown significant promise for reconstructing MR images from sparsely sampled k-space data using deep learning. In this work, we propose a technique that rapidly estimates deep neural networks directly at reconstruction time by fitting them on small adaptively estimated neighborhoods of a training set. In brief, our algorithm alternates between searching for neighbors in a data set that are similar to the test reconstruction, and training a local network on these neighbors followed by updating the test reconstruction. Because our reconstruction model is learned on a dataset that is structurally similar to the image being reconstructed rather than being fit on a large, diverse training set, it is more adaptive to new scans. It can also handle changes in training sets and flexible scan settings, while being relatively fast. Our approach, dubbed LONDN-MRI, was validated on the FastMRI multi-coil knee data set using deep unrolled reconstruction networks. Reconstructions were performed at four fold and eight fold undersampling of k-space with 1D variable-density random phase-encode undersampling masks. Our results demonstrate that our proposed locally-trained method produces higher-quality reconstructions compared to models trained globally on larger datasets.

Index Terms—Magnetic resonance imaging, machine learning, deep learning, unrolling, compressed sensing.

I. INTRODUCTION

In applications like X-ray computed tomography (CT) [1] and magnetic resonance imaging (MRI) [2], reconstructing images from undersampled or corrupted observations is of critical importance. For example, this is necessary to reduce a patient's exposure to radiation in CT or reduce time spent acquiring MRI data. MRI scans involve sequential data acquisition resulting in long acquisition times that are not

only a burden for patients and hospitals, but also make MRI susceptible to motion artifacts. Reconstructing images from limited measurements can speed up the MRI scan, but usually entails solving an ill-posed inverse problem. Recent approaches to accelerating MRI acquisition such as compressed sensing (CS) [3] reduce scan time by collecting fewer measurements while preserving image quality by exploiting image priors or regularizers. Historically, regularization in CS-MRI has been based on sparsity of wavelet coefficients [4] or using total variation [5]. While conventional CS assumes sparse or incoherent signals, approaches based on learned image models have been shown to be more effective for MRI reconstruction, starting with learned synthesis dictionaries [6], [7]. The dictionary parameters could be learned from unpaired clean image patches from a dataset and used for reconstruction or learned simultaneously with image reconstruction [6], [8], [9]. Additionally, recent advances in sparsifying transform learning have resulted in efficient or inexpensive data-adaptive sparsity-based reconstruction frameworks for MRI [10]–[12]. Other contemporary techniques could allow learning explicit regularizers in a supervised manner [13] for improved image restoration.

Convolutional neural networks have gained popularity in recent years as a result of the introduction of deep learning-based approaches for computer vision applications. They are now used for image denoising, classification, segmentation, and, more recently, medical image reconstruction. The U-net [14], [15] is a deep convolutional neural network (or CNN) that is frequently used in imaging applications. It has a contracting path for context acquisition and an expanding symmetric path for precise localization. There are numerous other network models available, including the Transformer architecture, which enables sharing of representations and feature transmission across multiple tasks in order to obtain higher-quality, super-resolved, and motion-artifact-free images from highly undersampled and degenerated MRI data [16]. Due to the popularity and computational efficiency of deep learning methodologies, there has been an increasing trend toward the use of deep supervised methods in MRI applications. MR image reconstruction techniques that are either supervised or unsupervised include image-domain (denoising) methods, sensor-domain methods, AUTOMAP, and hybrid-domain methods (cf. review in [11]). To improve stability

S. Liang is with the Department of Biomedical Engineering, Michigan State University, East Lansing, MI 48824 (liangs16@msu.edu).

A. Lahiri is with the Department of Electrical and Computer Engineering, University of Michigan, Ann Arbor, MI 48901 (anishl@umich.edu).

S. Ravishankar is with the Department of Computational Mathematics, Science and Engineering and the Department of Biomedical Engineering, Michigan State University, East Lansing, MI 48824 (ravisha3@msu.edu).

This work was supported in part by a research gift from the Advanced Radiology Services (ARS) Foundation.

and performance, hybrid-domain methods (e.g., [17]) enforce data consistency (i.e., the reconstruction is enforced to be consistent with the measurement model) all through training and reconstruction. Networks with data consistency layers play an important role in MR imaging to keep the reconstructed image consistent with the original image in k-space [18], [19]. These include deep unrolling-based methods [20], [21] (that unroll a traditional iterative algorithm and learn the regularization parameters therein), regularization by denoising [22], plug-and-play methods [23], etc. For example, Yang et al. [24] proposed ADMM-CSNet to learn the parameters of the ADMM algorithm via neural networks. ISTA-Net was similarly inspired by the Iterative Shrinkage-Thresholding Algorithm (ISTA) for optimizing a general ℓ_1 norm CS reconstruction model [25]. Moreover, transfer learning [26], a well-known technique, can also enable the use of neural networks for MRI reconstruction without a need for extensive datasets. While these CNN-based reconstruction methods have outperformed traditional compressed sensing (CS) methods, there remain concerns about their stability and interpretability [27].

Apart from algorithmic advances, another driving force behind deep learning-based reconstruction is the rapid growth of publicly available training datasets. The availability of (paired or unpaired) training data sets made possible by efforts like OCMR [28] and fastMRI [29] has enabled rapidly demonstrating the capacity of deep learning-based algorithms for improved image reconstruction or denoising quality in MRI applications. While many deep learning approaches are based on pixel-by-pixel supervised learning, they often require large, paired data sets and long training times to learn models with a large number of parameters. Some works have focused on unsupervised learning such as generative adversarial network (GAN)-based methods [30]–[32], but may still require large data sets. A recent deep learning-based approach is the deep image prior [33], which has been applied to MRI [34] and learns a neural network for reconstruction in an unsupervised fashion from a single image’s measurements. A related approach dubbed self-supervised learning has also shown promise for MRI [35] and uses a large unpaired data set.

A. Contributions

While deep learning approaches have gained popularity for MRI reconstruction due to their ability to model complex data sets, they often have difficulties generalizing to new data or distinct experimental situations at test time. Deep CNNs usually require enormous datasets to ensure adequate performance trade-offs. In this work, we propose to learn adaptive Local Neighborhood-based Networks for MRI (LOND-Net) reconstruction. The approach efficiently learns reconstruction networks from small clusters in flexible training sets and directly at reconstruction time. The models are trained using a small number of adaptively chosen neighbors that are in close proximity to (or are similar to in a sense) the underlying (to be reconstructed) image (cf. [36] for a slightly related approach in the context of patch-based dictionary learning). The proposed algorithm for image reconstruction alternates between finding a small set of similar images to a current reconstruction, and training the network locally on such neighbors and updating

the reconstruction. We show connections of this algorithm to a challenging bilevel optimization problem. The proposed local learning approach can be combined with any existing deep learning MRI framework to improve its performance (e.g., unrolled networks, image-domain denoisers such as the U-Net or DIDN, etc.). Through several experiments on the FastMRI data set, we demonstrate that the proposed learned model is extremely adaptable to individual scans as well as changes in experimental conditions (e.g., sampling masks), training set modifications, and so on. Our results show that the proposed local adaptation technique outperforms popular networks (e.g., the MoDL method [17]) trained on larger (global) datasets at a variety of MRI k-space undersampling factors. This work is a substantial extension of our very recent conference work [37] with comprehensive experiments and evaluations and theoretical understanding. To better understand the proposed model, we perform a variety of studies including on the effect of different similarity/distance metrics (e.g., euclidean or ℓ_2 distance, Manhattan or ℓ_1 distance, normalized cross-correlation), or weight regularization during learning, etc.

B. Organization

The rest of this article is organized as follows. Section II discusses some preliminaries on multi-coil MRI reconstruction and the approach for searching neighbors that will be used in our algorithm. Section III describes the proposed technique and its interpretations. Section IV presents the experimental setup and results. Section V provides a discussion of our findings, and in Section VI, we conclude.

II. PRELIMINARIES

A. Multi-coil MRI Reconstruction

When an image $\mathbf{x} \in \mathbb{C}^q$ (vectorized) is sufficiently sparse in some transform domain and the transform is sufficiently incoherent with the measurement operator, the theory of compressed sensing [3], [38] enables accurate image recovery from limited measurements. The image reconstruction problem in MRI is typically formulated as an optimization of a data-fidelity penalty and a regularizer as follows:

$$\hat{\mathbf{x}} = \arg \min_{\mathbf{x}} \sum_{c=1}^{N_c} \|\mathbf{A}_c \mathbf{x} - \mathbf{y}_c\|_2^2 + \lambda \mathcal{R}(\mathbf{x}), \quad (1)$$

where $\mathbf{y}_c \in \mathbb{C}^p$, $c = 1, \dots, N_c$, represent the acquired k-space measurements from N_c coils. We write the imaging forward operator or measurement operator as $\mathbf{A}_c = \mathbf{M} \mathcal{F} \mathbf{S}_c$, where $\mathbf{M} \in \{0, 1\}^{p \times q}$ is a masking operator that captures the undersampling pattern in k-space, $\mathcal{F} \in \mathbb{C}^{q \times q}$ is the Fourier transform operator (corresponding to densely sampled measurements), and $\mathbf{S}_c \in \mathbb{C}^{q \times q}$ is the c th coil-sensitivity matrix (a diagonal matrix). Additionally, the regularizer above may include a slew of terms capturing the assumed model of the underlying image. It enables enforcing desirable properties such as spatial smoothness, image sparsity, or edge preservation in the reconstructed image. Numerous iterative optimization techniques exist for (1). In MRI, the regularizer can involve ℓ_1 penalty on wavelet coefficients [4] or a total variation penalty [5] or patch-based sparsity in learned dictionaries [6]

or sparsifying transforms [12], or proximity to deep learning-based reconstructions, etc. For example, sparsity w.r.t. a known transform matrix \mathbf{W} is captured by $\mathcal{R}(\mathbf{x}) = \|\mathbf{W}\mathbf{x}\|_1$.

B. Neighbor Search

Our approach relies on finding images in a data set that are in a sense similar to the one being reconstructed. The similarity may be defined using a metric such as euclidean distance or other metrics. Assume we have a data set $\{\mathbf{x}_n, \mathbf{y}_n\}_{n=1}^N$ with N reference or ground-truth images \mathbf{x}_n and their corresponding k-space measurements \mathbf{y}_n (with multi-coil data), we use the distance metric d to find the k nearest neighbors to an (estimated/reconstructed) image \mathbf{x} as follows:

$$\hat{C}_x = \arg \min_{C \in \mathcal{C}, |C|=k} \sum_{r \in C} d(\mathbf{x}, \mathbf{x}_n), \quad (2)$$

where C is a set of cardinality k containing indices of feasible neighbors, and \mathcal{C} denotes the set of all such sets with k elements. Different distance functions could produce a different set of similar neighbors, which could then affect the outcome of the reconstruction algorithm, as our network modeling is dependent on the choice of the local data set. As a result, we used different metrics for evaluating our approach in this work. The distances serve as a proxy for data similarity, with nearby data considered similar and distant data considered dissimilar. We used the euclidean distance, Manhattan distance, and normalized cross-correlation as distance metrics as follows.

$$\begin{aligned} d^{L^1}(\mathbf{x}, \mathbf{x}_n) &= \|\mathbf{x} - \mathbf{x}_n\|_1 \\ d^{L^2}(\mathbf{x}, \mathbf{x}_n) &= \|\mathbf{x} - \mathbf{x}_n\|_2 \\ d^{NCC}(\mathbf{x}, \mathbf{x}_n) &= \frac{|\mathbf{x}^H \mathbf{x}_n|}{\|\mathbf{x}\|_2 \|\mathbf{x}_n\|_2} \end{aligned}$$

In all cases, we select the top k most similar neighbors from a set that correspond to the k smallest distances in (2). The indices of the chosen images are in the set \hat{C}_x , i.e., they are the minimizer in (2). These neighbors can be used to train the local model. These are expected to capture structures most similar to the image being reconstructed, enabling a highly effective reconstruction model to be learned.

III. PROPOSED LONDON-MRI ALGORITHM

Our primary objective is to learn an adaptive neural network for MRI reconstruction, in which the model's free parameters are fitted using training data that are similar in a sense to the current scan. We emphasize that the proposed model is local in the sense that it changes in response to the input. The advantage of the proposed method is that the model is fit for every scan and can thus be adaptive to the scan, handle changes in sampling masks, etc., readily.

The algorithm begins by obtaining an initial estimate of the underlying image, denoted \mathbf{x}^0 , from undersampled measurements \mathbf{y} . Our proposed strategy then alternates between computing the closest neighbors to the reconstruction in the training set and performing CNN-based supervised learning on the estimated local dataset. During supervised learning, the network weights could be randomly initialized or could be warm started with the weights of a pre-trained (e.g., state-of-the-art) network. In the latter case, the pre-trained network

would adapt to the features of images similar to the one being reconstructed (akin to transfer learning [26]). In each iteration, the nearest ground truth images in the training set are computed in relation to the reconstruction (estimate) predicted by the locally learned network, except in the first iteration, when the nearest neighbors are computed in relation to the (typically highly aliased) initial \mathbf{x}^0 (we used corresponding aliased images in the dataset for computing distances in the first iteration). In practice, pairwise distances to even a large number of images can be computed very efficiently (in parallel), after which the local network can be rapidly learned on a small set of neighbors (typically a shallow network or with early stopping). The network weights for deep reconstruction are constantly updated to map the initial images for the local data set to the target (ground truth) versions.

To demonstrate our approach, we used the state-of-the-art deep CNN reconstruction model MoDL [17], which is trained locally in our scheme. Additionally, we trained it globally, i.e., once on a larger dataset, in order to compare it to our on-the-fly neighborhood-based learning scheme. For completeness, we briefly recap the MoDL scheme in the following and discuss its local training within our framework. MoDL is similar to the plug-and-play approach, except that instead of pre-trained denoiser networks, end-to-end training is used to learn the shared network weights across iterations in the architecture.

A. Network Model and Training

The proposed approach is compatible with any network architecture. We use MoDL, which has shown promise for MR image reconstruction, and combines a denoising network with a data consistency (DC) module in each iteration of an unrolled architecture. MoDL unrolls alternating minimization for the following problem:

$$L_a(\mathbf{z}, \mathbf{x}) := \nu \sum_{c=1}^{N_c} \|\mathbf{A}_c \mathbf{x} - \mathbf{y}_c\|_2^2 + \mathcal{R}(\mathbf{z}) + \mu \|\mathbf{x} - \mathbf{z}\|_2^2. \quad (3)$$

We denote the initial image in the process as \mathbf{x}^0 , $\nu \geq 0$ weights the data-consistency term above, and $\mu \geq 0$ weights the proximity of \mathbf{x} to \mathbf{z} . By decomposing the optimization into two subproblems over \mathbf{z} and \mathbf{x} , the explicit regularizer-based update for \mathbf{z} can be solved by replacing it with a CNN-based denoiser ($D_\theta(\cdot)$), and the denoised estimate is then used to update \mathbf{x} . The \mathbf{x} update in the MoDL scheme involves the data-consistency term and is performed using Conjugate Gradient (CG) descent. Thus, \mathbf{z} is obtained as the output from a CNN-based denoiser (D_θ) and \mathbf{x} is updated by CG. This alternating scheme is repeated L times (unrolling), with the initial input image \mathbf{x}^0 being passed through L blocks of denoising CNN + CG updates. Now, if $\mathbf{S}_\theta^l(\cdot)$ is the function capturing the l th iteration of the algorithm, then the MoDL output for the l th block is given as

$$\begin{aligned} \mathbf{x}^{l+1} &= \mathbf{S}_\theta^l(\mathbf{x}^l) = \mathbf{S}(\mathbf{x}^l, \theta, \nu_l, \{\mathbf{A}_c, \mathbf{y}_c\}_{c=1}^{N_c}), \text{ and} \\ \mathbf{S}(\bar{\mathbf{x}}, \theta, \nu, \{\mathbf{A}_c, \mathbf{y}_c\}_{c=1}^{N_c}) &\triangleq \\ \arg \min_{\mathbf{x}} \nu \sum_{c=1}^{N_c} \|\mathbf{A}_c \mathbf{x} - \mathbf{y}_c\|_2^2 &+ \|\mathbf{x} - D_\theta(\bar{\mathbf{x}})\|_2^2. \end{aligned} \quad (4)$$

After L iterations, the final output is

$$\mathbf{x}_{\text{supervised}} = \mathbf{x}^L = \left(\bigcirc_{l=0}^{L-1} \mathcal{S}_\theta^l \right) (\mathbf{x}^0) \triangleq \mathcal{M}_\theta(\mathbf{x}^0), \quad (5)$$

where $\bigcirc_{i=0}^{L-1} f^i$ represents the composition of L functions $f^{L-1} \circ f^{L-2} \circ \dots \circ f^0$, and \mathbf{x}^0 is the initial image. The weights of the denoiser \mathcal{D}_θ are shared across the L blocks. The network parameters θ are learned in a supervised manner so that $\mathbf{x}_{\text{supervised}}$ matches known ground truths (in mean squared error or other metric) on a (large/global or local) training set. This involves the following optimization for training:

$$\begin{aligned} \hat{\theta} &= \arg \min_{\theta} \sum_{n \in S} C_\beta(\mathcal{M}_\theta(\mathbf{x}_n^0); \mathbf{x}_n) \\ &= \arg \min_{\theta} \sum_{n \in S} (\|\mathbf{x}_n - \mathcal{M}_\theta(\mathbf{x}_n^0)\|_2^2), \end{aligned}$$

where n indexes the samples from the data set used for training, with \mathbf{x}_n denoting the n th target (or ground truth) image reconstructed from fully-sampled k-space measurements and \mathbf{x}_n^0 denotes the initial image estimate from undersampled measurements. The cost $C_\beta(\hat{\mathbf{x}}_n; \mathbf{x}_n)$ denotes the training loss. The main difference between a globally learned and locally learned network is the choice of the set S of training indices. For the proposed local approach, we fit the network based on the k training samples closest to the current test image estimate, whereas the conventional (or global) training would fit networks to a large dataset. The initial image estimate \mathbf{x}_n^0 is obtained from the undersampled measurements \mathbf{y}_n by e.g., using a simple analytical reconstruction scheme such as applying the adjoint of the forward model to the measurements.

In each iteration, the network is updated (Fig. 1), and the initial estimate of the underlying unknown image is passed through the network to obtain a new estimate. In Fig. 1, we illustrate the iterative process of neighbor fine-tuning and local network updating. Local learning may have the advantage of accommodating changes in experimental conditions (e.g., undersampling pattern) at test time, provided that such modified measurements and initial images for the small local training set can be easily simulated from the existing \mathbf{x}_n or \mathbf{y}_n . Our overall algorithm is also summarized in Algorithm 1.

B. Regularization

In order to avoid over-fitting when training networks on small sets, we also adopted regularization of weights during training as follows:

$$\hat{\theta} = \arg \min_{\theta} \sum_{n \in S} \|\mathbf{x}_n - \mathcal{M}_\theta(\mathbf{x}_n^0)\|_2^2 + \lambda \mathcal{R}(\theta), \quad (6)$$

where $\mathcal{R}(\cdot)$ denotes the regularization term on network weights. We primarily used the ℓ_1 norm regularizer to enforce sparsity of the network weights to learn simpler models. We observed that regularizing the local model enables it to converge more easily, and shrinks weights for less important or noisy features to zero. We provide more discussion in the experiments section.

Algorithm 1 LOND-N-MRI Algorithm

Require: Initial image \mathbf{x}^0 , number of neighbors k , k-space undersampling mask \mathbf{M} , regularization parameters ν and μ , number of training epochs T , number of iterations of alternating algorithm S .

- 1: Initialize reconstruction network parameters θ with pre-learned network weights $\hat{\theta}$ or randomly initialized weights. Set $\mathbf{x} = \mathbf{x}^0$.
- 2: **for** Iteration < maximal iteration S **do**
- 3: Compute the set of k similar neighbors $\hat{C}_\mathbf{x}$ to the current reconstruction estimate \mathbf{x} using metric d .
- 4: **for** epoch < maximal number T **do**
- 5: For each batch of neighbor data, compute the gradient of the training loss with respect to network parameters θ and make a step of update of the parameters.
- 6: **end for**
- 7: Update $\mathbf{x} \leftarrow \mathcal{M}_\theta(\mathbf{x}^0)$
- 8: **end for**
- 9: **return** reconstruction \mathbf{x} and learned net. parameters θ .

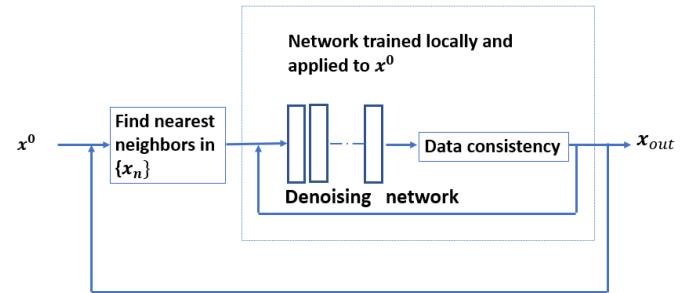


Fig. 1: Flowchart of the proposed LOND-N-MRI scheme with a specific unrolled reconstruction network. The denoising network could be for example a U-Net or the recent DIDN.

C. Connections to Bilevel Optimization

The alternating algorithm for training involving a neighbor search step and a local network update step could be viewed as a heuristic algorithm for the following bilevel optimization problem:

$$\begin{aligned} \min_{C \in \mathcal{C}, |C|=k} \sum_{i \in C} \|f_{\theta(C)}(\mathbf{y}) - \mathbf{x}_i\|_2^2, \\ \text{s.t. } \theta(C) = \arg \min_{\theta} \sum_{i \in C} \|\mathbf{x}_i - f_{\theta}(\mathbf{y}_i)\|_2^2. \end{aligned} \quad (7)$$

Here, $f_{\theta(C)}$ denotes a deep neural network learned on a subset C of a data set that maps the current k-space measurements \mathbf{y} to a reconstruction. The network is akin to $\mathcal{M}_\theta(\mathbf{x}^0)$ shown earlier, but with \mathbf{x}^0 assumed to be generated from \mathbf{y} (e.g., via the well-known sum of squares of coil-wise inverse Fourier transforms, or via SENSE reconstruction, etc.). Problem 7 aims to find the best neighborhood or cluster among the training data, where the reconstructed image belongs (with closest distances to neighbors – we assumed euclidean distance here), with the network weights for reconstruction estimated on the data in that cluster. Problem 7 is a bilevel optimization

problem with the cluster optimization forming the upper level cost and network optimization forming the lower level cost. Bilevel problems are known to be quite challenging [13], [39]. It is also a combinatorial problem because we would have to sweep through all possible choices of clusters of k training samples with reconstruction networks trained in each such cluster, to determine the best cluster choice.

The proposed algorithm is akin to optimizing the bilevel problem by optimizing for the network weights θ with the clustering C fixed (the lower level problem) and then optimizing for the clustering C (upper level minimization) with the network weights fixed. This is a heuristic because the optimized variables in each step are related, however, such an approach has been used in prior work [9] and shown to be approximately empirically convergent for the bilevel cost. In this work, we performed an empirical evaluation of convergence in the experiments section, where the alternating algorithm is shown to reduce the upper-level cost in (7).

IV. EXPERIMENTS

A. Experimental Framework

We evaluate the proposed LONDN-MRI reconstruction method on the multi-coil FastMRI knee dataset [29], [40]. We chose a random subset of 3000 images from the dataset as a training set and used 15 randomly selected unrelated images for testing. In some experiments, we evaluated the effect of training set size, where we worked with fewer images in the training set. Coil sensitivity maps for model-based reconstruction were generated for each scan using the BART toolbox [41] using fully-sampled k-space data.

Since the proposed LONDN-MRI framework is quite general and can be combined with any supervised deep learning based reconstruction approach, we chose the recent popular model-based deep learning (MoDL) reconstruction network and compared globally (over the large set of training samples) and locally (over very small matched set of samples) learned versions of the model for different choices of deep denoisers in the network.¹ We performed reconstructions at fourfold or 4x acceleration (25.0% sampling) as well as at eightfold or 8x acceleration (12.5% sampling) of the k-space acquisition. In all cases, variable density 1D random Cartesian (phase-encode) undersampling of k-space was performed. The initial image estimates for MoDL were obtained by applying the adjoint of the measurement operator to the subsampled k-space data, and were then used to train both local and global versions of MoDL networks. In our local versions (LONDN-MRI), we used 30 images for training (searched from e.g., 3000 images). while the global versions used the full subset of training images.

B. Sampling Masks

We used binary masks for fourfold and eightfold Cartesian undersampling of k-space. Fig. 2 shows the sampling masks primarily used in our experiments that include a fully-sampled central region (with 31 central lines at 4x acceleration and

15 central lines at 8x acceleration) and the remaining phase encode lines were sampled uniformly at random.

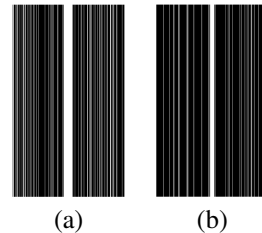


Fig. 2: Undersampling masks used in our experiments: (a) fourfold undersampled 1D Cartesian phase-encoded; and (b) eightfold undersampled 1D Cartesian phase-encoded. The masks were zero-padded for slightly larger images.

C. Performance Metrics

We used three common metrics to quantify the reconstruction quality of different methods. These were the peak signal-to-noise ratio (PSNR) in decibels (dB), structural similarity index (SSIM) [42], and the high frequency error norm (HFEN) [6], which were computed between the reconstruction and the ground truth obtained from fully-sampled k-space data. The HFEN was computed from the ℓ_2 norm of the difference between Laplacian of Gaussian (LoG) filtered reconstructed and ground truth images. This was normalized by the ℓ_2 norm of the LoG filtered ground truth.

D. Network Architectures and Training

We trained two types of MoDL models at 4x and 8x k-space undersampling, respectively. One used the well-known UNet denoiser, with a two-channel input and two-channel output, where the real and imaginary parts of an image are separated into two channels. The network weights during training were initialized randomly (normally distributed). The ADAM optimizer was utilized for training the network weights. For LONDN-MRI, we used an initial learning rate of 6×10^{-5} with a multi-step learning rate scheduler, which decreases the learning rate at 100 and 150 epochs with learning rate decay 0.65. For training globally, we used an initial learning rate of 1×10^{-4} with 150 epochs of training and a multi-step learning rate scheduler that decreased the learning rate at 50 and 100 epochs with learning rate decay 0.6. For LONDN-MRI, MoDL with 5 iterations was used with a shallow UNet that had 2 layers in the encoder and decoder, respectively. We used a shallow network with dropout for the local model to avoid over-fitting to the very small training set. For the MoDL network trained globally (on large dataset) for making comparisons with, we utilized 4 layers in the decoder and encoder in UNet and 6 MoDL blocks. We used a batch size of 2 during training for both the global and local cases. Furthermore, for the data-consistency term, we used a tolerance of 10^{-5} in CG and a μ/ν ratio of 0.1. Also, we chose the regularization weight λ as 10^{-9} for LONDN-MRI, unless specified otherwise.

For the second MoDL architecture, we used the recent state-of-the-art denoising network DIDN [43], [44]. Due to the high complexity of the DIDN network, we first pre-trained

¹See https://github.com/sjames40/Multi_coil_local_model for our code in PyTorch.

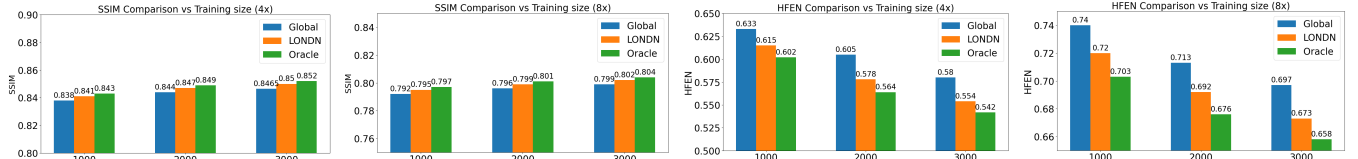


Fig. 3: Comparison of MoDL with UNet denoiser trained globally vs. using the proposed LONDON-MRI scheme(1 iteration). Reconstruction metrics are shown across training set sizes at 4x and 8x undersampling.

it on the larger (global) dataset (learning rate, etc., similar to the UNet case) before adapting the weights within LONDON-MRI for each scan. This is an alternative to constructing shallower versions of a network for local adaptation. The ADAM optimizer was utilized for training, with a learning rate of 5×10^{-5} in LONDON-MRI. We used 6 iterations of MoDL with the DIDN denoiser for which we used 3 down-up blocks (DUBs). The number of epochs for training was 30 in LONDON-MRI. The remaining training parameters were chosen similarly as in the previous UNet-based case. Using a pre-trained state-of-the-art denoiser allows the local adaptation to converge faster.

E. Results for the UNet-based Reconstructor

Table I compares the average PSNR values for reconstruction over the testing set at both 4x and 8x undersampling. We varied the number of images in the training set for a more comprehensive study. For LONDON-MRI, we used NCC to measure distances for neighbor search. We compare learning networks over a small set of similar images to learning networks over the larger datasets (global), as well as to an oracle LONDON scheme, where the neighbors in the training set were computed based on each ground truth test image. The oracle scheme would ideally provide an upper bound on the performance of the iterative LONDON-MRI scheme.

When varying the size of the training set, the global approach was trained on the full set each time, whereas the local approach performed training on small subsets of 30 training pairs selected from the larger datasets. The iterations of the LONDON-MRI scheme quickly improve reconstruction performance, and even with only 2 alternations, the PSNR values begin approaching the oracle setting. The LONDON schemes (oracle or iterative) consistently outperform the globally trained networks across the different training set sizes considered. Figure 3 compares the SSIM and HFEN reconstruction metrics using bar graphs, where a similar trend is observed as with PSNR.

Figs. 4 and 5 show images reconstructed by different methods at 8x and 4x undersampling, respectively. The LONDON-MRI reconstructions (either iterative or oracle) show less artifacts and sharper features and less errors than the global MoDL and initial aliased reconstructions. The iterative LONDON-MRI results are also quite close to the oracle result.

F. Performance with Different Distance Metrics

Here, we study the effect of different distance metrics for selecting the matching dataset for training in LONDON-MRI (oracle scheme). We tested the performance of MoDL with UNet denoiser using L1, L2, and normalized cross-correlation

Acceleration	Data Size	Global	LONDON-MRI (1 iteration)	LONDON-MRI (2 iterations)	Oracle
4x	1000	32.63	32.78	32.87	32.99
	2000	33.00	33.28	33.31	33.35
	3000	33.17	33.46	33.51	33.54
8x	1000	29.78	30.15	30.26	30.34
	2000	30.21	30.53	30.58	30.64
	3000	30.47	30.76	30.80	30.85

TABLE I: Average reconstruction PSNRs (in dB) for 15 images at 4x and 8x k-space undersampling. The proposed LONDON-MRI (with 1 or 2 alternations) is compared to training a global reconstructor for different training set sizes. We also compare to an oracle local reconstructor, where neighbors are found with respect to known ground truth test images.

Acceleration	Reconstruction Metric	L1	L2	NCC
4x	SSIM	0.85	0.849	0.852
	PSNR (dB)	33.49	33.44	33.54
	HFEN	0.552	0.56	0.542
8x	SSIM	0.803	0.802	0.804
	PSNR (dB)	30.79	30.71	30.85
	HFEN	0.664	0.674	0.658

TABLE II: Average PSNR, SSIM, and HFEN values over 15 testing images for LONDON-MRI with neighbor search performed using L1 distance, L2 distance, and normalized cross-correlation (NCC).

(NCC) for finding the matched training set from 3000 images. From the results in Table II, we see that the different distance functions offer slight differences in reconstruction performance, with NCC offering the best results with respect to all reconstruction metrics.

G. Results for the DIDN-based Reconstructor

Table III compares reconstruction performance on the test set with the DIDN denoiser-based MoDL architecture. Average PSNR values with LONDON-MRI are compared to those with networks trained globally at different training set sizes. We ran only 1 iteration of LONDON-MRI, where the reconstruction with a pre-trained (global) network was used to find neighbors for local adaptation (or local transfer). PSNR values for the oracle LONDON-MRI reconstructor are also shown. The overall performances with the DIDN-based architectures are better than with the UNet-based unrolled networks. The PSNRs for LONDON-MRI are consistently and similarly better than for the globally trained network across the different training set sizes considered, indicating potential for LONDON-MRI in improving more state-of-the-art models via local adaptation. Fig. 6 visually compares reconstructions and reconstruction errors (in zoomed in region) for different methods. We can see that the LONDON reconstructors capture the original image features

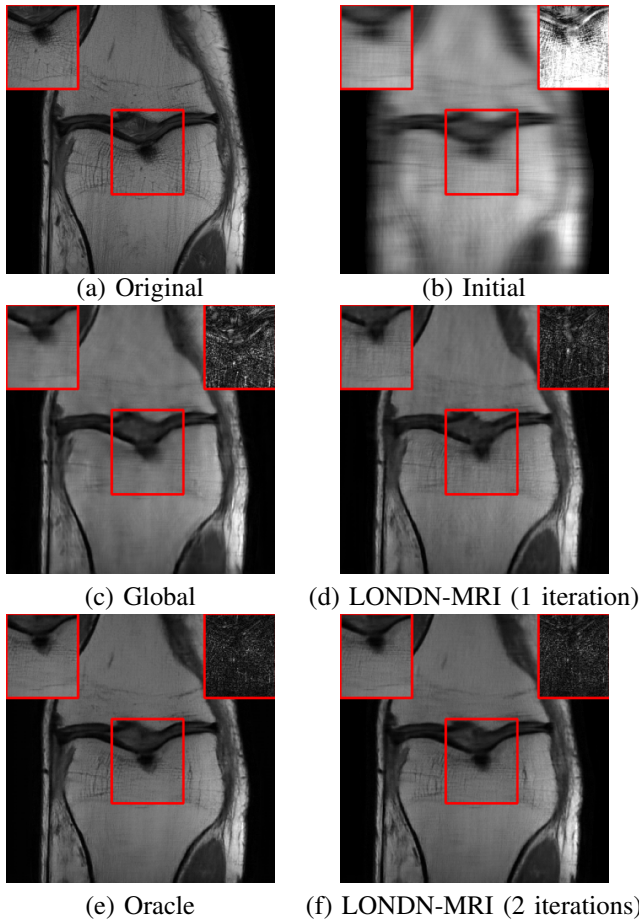


Fig. 4: Comparison of image reconstructions at 8x undersampling using MoDL architecture with UNet denoiser with 1000 training images: (a) ground truth, (b) initial image input to the networks (PSNR = 16.43 dB), (c) global reconstruction (PSNR = 29.26 dB), (d) LONDN-MRI (1 iteration) reconstruction (PSNR = 29.50 dB), (e) oracle LONDN-MRI reconstruction (PSNR = 29.72 dB), where the nearest neighbors in the training set are found using known ground truth test image, and (f) LONDN-MRI (2 iterations) reconstruction (PSNR = 29.68 dB). The inset panel on the top left in each image corresponds to a section of interest in the image (shown by the red bounding box), while the inset panel on the top right corresponds to the error map with respect to the ground truth.

better and sharper than the globally learned reconstructor.

H. Effect of Varying Scan Settings at Test Time

Since the reconstruction network in LONDN-MRI is trained for each scan, we would like to understand better the benefits this provides in terms of letting the network adapt to distinct scan settings.

So we chose the MoDL reconstructor with UNet denoiser (with same hyperparameters for training as before) and trained it on the 3000 image set in two ways: with a fixed sampling mask across the images (the mask was padded with zeros to account for slight variations in matrix sizes), and with a different random sampling mask for each image. The first setting was used in previous subsections. For LONDN-MRI, here, we used a different random sampling mask for each test scan, but the network was adapted locally with the same mask

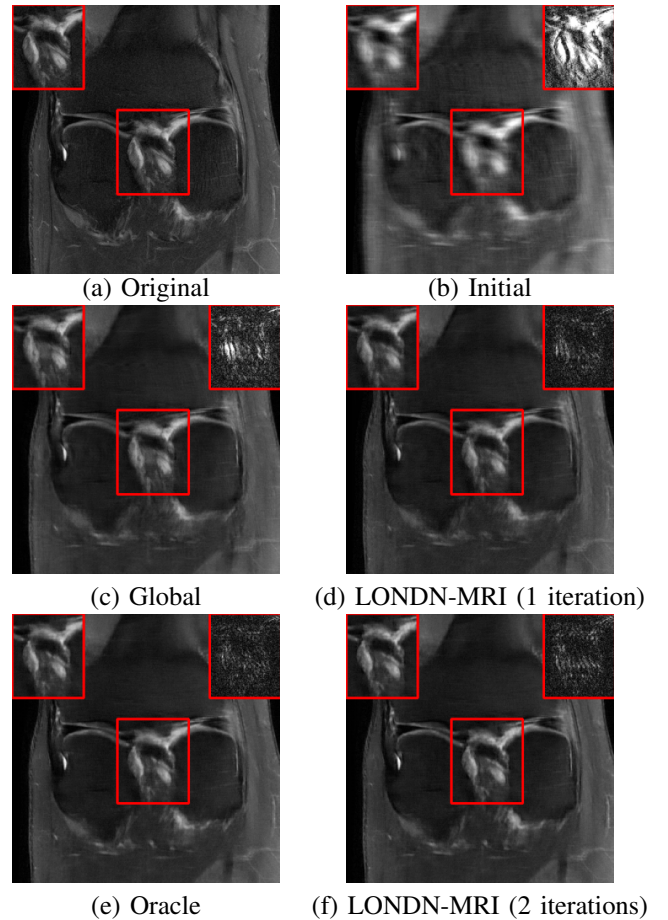


Fig. 5: Comparison of image reconstructions at 4x undersampling using MoDL architecture with UNet denoiser with 3000 training images: (a) ground truth and (b) initial image input to the networks (PSNR = 21.23 dB), (c) global reconstruction (PSNR = 32.78 dB), (d) LONDN-MRI (1 iteration) reconstruction (PSNR = 33.16 dB), (e) oracle LONDN-MRI reconstruction (PSNR = 33.30 dB), where the nearest neighbors in the training set are found using known ground truth test image, and (f) LONDN-MRI (2 iterations) reconstruction (PSNR = 33.25 dB). The inset panel on the top left in each image corresponds to a section of interest in the image (shown by the red bounding box in the image), while the inset panel on the top right corresponds to the error map with respect to the ground truth.

used across each (small) local training set. Table IV shows the average PSNR values on the test set with these different strategies as well as with the oracle LONDN-MRI scheme. It is clear that the globally learned model with a fixed sampling mask struggles to generalize to the different scan settings at test time. But training the global model with random sampling masks leads to improved reconstruction PSNRs. Importantly, the LONDN-MRI schemes that adapt the reconstruction model to the settings as well as the data for each scan provide marked improvements over both globally learned network settings.

I. Effect of Weight Regularization in LONDN-MRI

Here, we vary the strength of the regularization penalty weight in (6) and run LONDN-MRI over the test set at 4x k-space undersampling. Fig. 7 plots the average PSNR as a

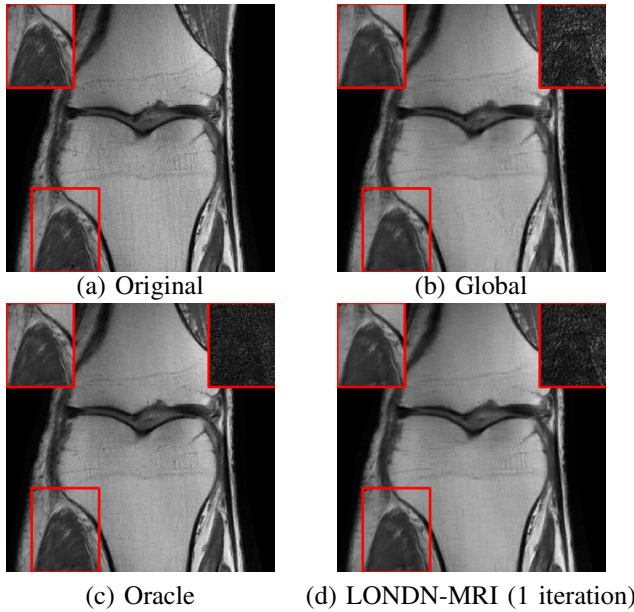


Fig. 6: Comparison of image reconstruction at 4x undersampling for the MoDL network with DIDN denoiser and 3000 training images: (a) ground truth, (b) global MoDL reconstruction (PSNR = 34.15 dB), (c) LONDN-MRI (1 iteration) reconstruction (PSNR = 34.45 dB), and (d) oracle LONDN-MRI reconstruction (PSNR = 34.54 dB), where the nearest neighbors in the training set are found using the ground truth test image. The inset panel on the top left in each image corresponds to a region of interest (shown by red bounding box in the image), and the inset panel on the top right corresponds to the error map with respect to the ground truth.

Acceleration	Data Size	Global	LONDN-MRI (1 iteration)	Oracle
4x	1000	33.66	33.92	33.96
	2000	34.01	34.23	34.31
	3000	34.15	34.39	34.42
8x	1000	31.02	31.33	31.37
	2000	31.34	31.64	31.68
	3000	31.79	32.08	32.12

TABLE III: Average reconstruction PSNR values (in dB) on the testing set at 4x and 8x undersampling for various training set sizes. MoDL reconstructor with DIDN denoiser is used.

Acceleration	Global Model trained with a fixed mask	Global Model trained with rand. masks	LONDN-MRI (2 iterations)	Oracle LONDN
4x	33.03	33.19	33.56	33.64
8x	30.62	30.84	31.14	31.22

TABLE IV: Average reconstruction PSNR values (in dB) on the test set at 4x and 8x undersampling. The LONDN-MRI results are compared to training a global model with a fixed sampling mask or with random masks.

function of the penalty weight for the MoDL network with UNet denoiser. The normalized cross-correlation distance was used during neighbor search, with other parameters as before. The result shows slight benefits for choosing the regularization

weight carefully.

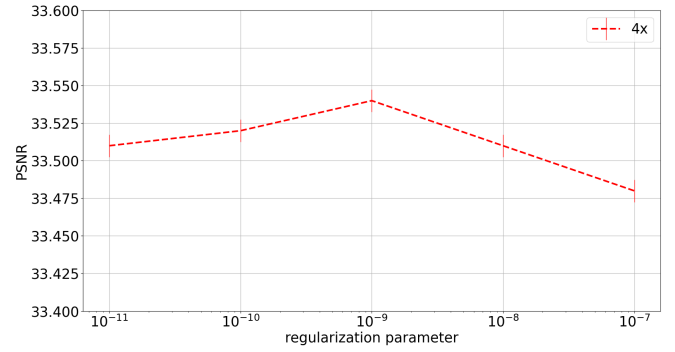


Fig. 7: Average reconstruction PSNR on the test set at 4x undersampling for different regularization penalty parameters. We used ℓ_1 norm regularization of network weights for an MoDL network with UNet denoiser.

J. Evaluating the Accuracy of Neighbor Search

Here, we study how the neighbor search proceeds across the iterations or alternations of LONDN-MRI. We are interested to know if our locally learned reconstructor can improve the neighbor finding process over iterations. We used all images from the test set. First, we find the k closest neighbors (in terms of euclidean distance) for each ground truth test image amongst the ground truth training image. The set C_r^* contains the indices of these *oracle* neighbors for a test image indexed r . The set \hat{C}_r contains the indices of closest neighbors from a certain iteration of LONDN-MRI. The neighbor matching accuracy (NMA) metric below computes the average (over the test set indices \mathcal{T}) percentage match between the two sets:

$$\text{NMA} := \frac{100}{|\mathcal{C}|} \sum_{r \in \mathcal{T}} \frac{|\hat{C}_r \cap C_r^*|}{k}, \quad (8)$$

The accuracy of the neighbor search at both 4x and 8x undersampling is shown in Fig. 8. The accuracy of the initial search (based on x^0) and after 1 or 2 iterations of LONDN-MRI are shown. We find nearest neighbors for the initial highly

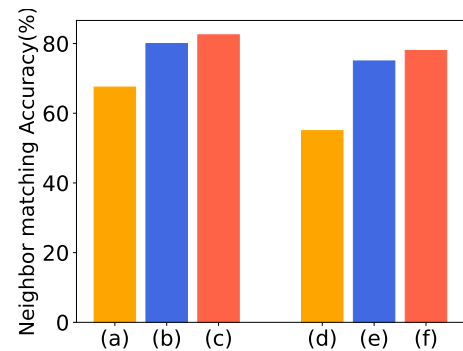


Fig. 8: Average accuracy (over test set) of neighbor search in LONDN-MRI (MoDL with UNet denoiser) at 4x undersampling in (a) the first iteration (neighbors found with respect to the initial input images x^0) and after the (b) first and (c) second iteration. (d)-(f) are corresponding results at 8x undersampling.

aliased x^0 with respect to the corresponding aliased images in the training set (based on the same k-space undersampling mask as at testing time), rather than based on the ground truth training images, because the latter resulted in lower neighbor search accuracy for x^0 . It is clear from Fig. 8 that the accuracy improves quickly and tapers off in few iterations.

K. Convergence of Loss in Bilevel Optimization

Finally, we study the behavior of the alternating LOND-N-MRI algorithm as a heuristic for the bilevel optimization formulation in (7). Here, we used an MoDL network with the UNet denoiser and $k = 30$ training pairs were chosen (from 3000 cases) in the local dataset in each iteration of LOND-N-MRI. The UNet weights were randomly initialized to begin with, and the neighbor search in the first iteration of LOND-N-MRI was performed using x^0 and correspondingly generated aliased training images. Fig. 9 plots the upper level loss in (7) (in a root mean squared error form) after each iteration of LOND-N-MRI for a test image. Here, we ran many iterations to verify convergence. We observe that the loss changes very little after a few iterations and stabilizes. This matches with the behavior of the neighbor search accuracy bar plots. The result indicates that the proposed alternating scheme could be a reasonable heuristic for reducing the loss in the challenging problem (7). Finally, we compare the loss values in Fig. 9 with an oracle loss, where the upper level loss in (7) is computed using the ground truth test image and its k nearest neighbors. It is clear that the loss values in LOND-N-MRI converge very close to the oracle loss, indicating potential for our scheme.

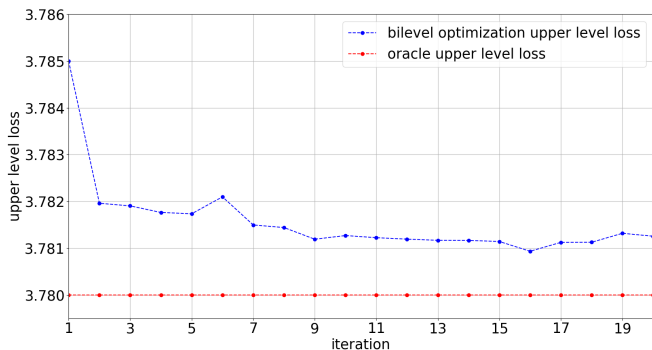


Fig. 9: Upper level loss in the bilevel optimization formulation (7) plotted over the iterations (after network update step) of the LOND-N-MRI scheme at 4x undersampling. We used MoDL with a UNet denoiser and $k = 30$ for neighbor search. In addition, the red line shows an oracle upper level loss computed using the ground truth test image and its k nearest neighbors.

V. DISCUSSION

We proposed a novel LOND-N-MRI reconstruction technique that efficiently matches test reconstructions to a cluster of a dataset, where networks are adaptively estimated on images most related to a current scan. Our results on the multi-coil FastMRI dataset showed promise for our scan or patient adaptive network estimation scheme. The approach does not

involve pre-training and can thus readily handle changes in the training set. The networks in LOND-N-MRI can be randomly initialized and trained adaptively on very small datasets, and such networks outperformed models trained globally on much larger datasets (with lengthy training times). For example, LOND-N-MRI with 2 alternations involving MoDL with a randomly initialized UNet denoiser took 30 minutes to complete on a NVIDIA GeForce RTX 3080 GPU (with batchsize of 2 and 200 epochs each time to update networks locally), whereas the global MoDL training on 3000 images with 150 epochs of ADAM optimizer took about 69 hours. LOND-N-MRI requires only a few images (e.g., 30) to train networks, with often 200-250 epochs for locally updating randomly initialized networks such as the UNet. Fewer epochs (often 10 suffices) of update were needed with pre-trained networks such as the pre-trained DIDN, resulting in runtimes of only 3 minutes for 1 iteration of LOND-N-MRI. Although our approach is iterative, we found that even a couple iterations are sufficient to provide image quality close to the oracle case. The rapid convergence was also seen in the convergence of neighbor search accuracy and the loss in the underlying bilevel optimization. The use of only few iterations of LOND-N-MRI and a small local dataset (as well as pre-training) reduces the computational cost of our scheme, given that models need to be updated for each scan.

When compared to the supervised global model, the proposed method offers consistently improved reconstruction quality in terms of PSNR, SSIM, and HFEN metrics. Additionally, we demonstrated that the local model is easily adaptable to test time scan changes, such as changes to the sampling mask, compared to a globally learned model, which is fixed once learned. Our approach produced comparable improvements over the global scheme, when using a small dataset (1000 cases) or a relatively larger set (3000 cases). Additionally, our study with different distance metrics revealed they have some effect on network reconstruction performance. The NCC metric provided the best reconstruction quality. This also indicates that perhaps a learned metric [45] could further enhance the performance of LOND-N-MRI.

VI. CONCLUSIONS

This paper examined supervised learning of deep unrolled networks at reconstruction time for MRI by exploiting training sets along with local modeling and clustering. We showed advantages for this approach at different k-space undersampling factors over networks learned in a global manner on larger data sets. The training may be connected to a bilevel optimization problem. We also compared different distance metrics for finding neighbors in our approach and regularization to reduce local overfitting. We intend to expand our approaches in the future by incorporating non-Cartesian undersampling patterns, such as radial and spiral patterns, as well as deploy to other imaging modalities. Additionally, the method's generalizability will be examined, with a particular emphasis on heterogeneous datasets. We showed benefits for both randomly seeded training of simple models and for transfer learning of sophisticated pre-trained models, and believe our methodology could be applied to a variety of deep learning-based tasks effectively

to improve overall performance. Finally, metric learning [45] to improve local clustering and subsequent network adaptation will be an important future direction.

REFERENCES

- [1] I. A. Elbakri and J. A. Fessler, "Statistical image reconstruction for polyenergetic X-ray computed tomography," *IEEE Transactions on Medical Imaging*, vol. 21, no. 2, pp. 89–99, 2002.
- [2] J. A. Fessler, "Model-Based Image Reconstruction for MRI," *IEEE Signal Processing Magazine*, vol. 27, no. 4, pp. 81–89, 2010.
- [3] D.L. Donoho, "Compressed sensing," *IEEE Transactions on Information Theory*, vol. 52, no. 4, pp. 1289–1306, 2006.
- [4] M. Kivanc Mihcak, I. Kozintsev, K. Ramchandran, and P. Moulin, "Low-complexity image denoising based on statistical modeling of wavelet coefficients," *IEEE Signal Processing Letters*, vol. 6, no. 12, pp. 300–303, 1999.
- [5] S. Ma, W. Yin, Y. Zhang, and A. Chakraborty, "An efficient algorithm for compressed MR imaging using total variation and wavelets," in *2008 IEEE Conference on Computer Vision and Pattern Recognition*, 2008, pp. 1–8.
- [6] S. Ravishankar and Y. Bresler, "MR image reconstruction from highly undersampled k-space data by dictionary learning," *IEEE Transactions on Medical Imaging*, vol. 30, no. 5, pp. 1028–1041, 2011.
- [7] S. G. Lingala and M. Jacob, "Blind compressive sensing dynamic MRI," *IEEE Transactions on Medical Imaging*, vol. 32, no. 6, pp. 1132–1145, 2013.
- [8] Q. Xu, H. Yu, X. Mou, L. Zhang, J. Hsieh, and G. Wang, "Low-dose x-ray ct reconstruction via dictionary learning," *IEEE Transactions on Medical Imaging*, vol. 31, no. 9, pp. 1682–1697, 2012.
- [9] Siqi Ye, Zhipeng Li, Michael T. McCann, Yong Long, and Saiprasad Ravishankar, "Unified Supervised-Unsupervised (SUPER) Learning for X-Ray CT Image Reconstruction," *IEEE Transactions on Medical Imaging*, vol. 40, no. 11, pp. 2986–3001, 2021.
- [10] S. Ravishankar and Y. Bresler, "Learning sparsifying transforms," *IEEE Transactions on Signal Processing*, vol. 61, no. 5, pp. 1072–1086, 2012.
- [11] S. Ravishankar, J. C. Ye, and J. A. Fessler, "Image reconstruction: From sparsity to data-adaptive methods and machine learning," *Proceedings of the IEEE*, vol. 108, no. 1, pp. 86–109, 2020.
- [12] B. Wen, S. Ravishankar, L. Pfister, and Y. Bresler, "Transform learning for magnetic resonance image reconstruction: From model-based learning to building neural networks," *IEEE Signal Processing Magazine*, vol. 37, no. 1, pp. 41–53, 2020.
- [13] A. Ghosh, M.T. Mccann, and S. Ravishankar, "Bilevel learning of l1 regularizrs with closed-form gradients (blorc)," in *ICASSP 2022 - 2022 IEEE International Conference on Acoustics, Speech and Signal Processing (ICASSP)*, 2022, pp. 1491–1495.
- [14] O. Ronneberger, P. Fischer, and T. Brox, "U-net: Convolutional networks for biomedical image segmentation," in *Medical Image Computing and Computer-Assisted Intervention – MICCAI 2015*, 2015, pp. 234–241.
- [15] K. H. Jin, M. T. McCann, E. Froustey, and M. Unser, "Deep convolutional neural network for inverse problems in imaging," *IEEE Trans. Im. Proc.*, vol. 26, no. 9, pp. 4509–22, Sept. 2017.
- [16] C. Feng, Y. Yan, H. Fu, L. Chen, and Y. Xu, "Task Transformer Network for Joint MRI Reconstruction and Super-Resolution," in *International Conference on Medical Image Computing and Computer Assisted Intervention (MICCAI)*, 2021.
- [17] H. K. Aggarwal, M. P. Mani, and M. Jacob, "MoDL: model-based deep learning architecture for inverse problems," *IEEE Trans. Med. Imaging*, vol. 38, no. 2, pp. 394–405, 2019.
- [18] H. Zheng, F. Fang, and G. Zhang, "Cascaded dilated dense network with two-step data consistency for MRI reconstruction," in *NeurIPS*, 2019.
- [19] J. Schlemper, J. Caballero, J. V. Hajnal, A. Price, and D. Rueckert, "A Deep Cascade of Convolutional Neural Networks for Dynamic MR Image Reconstruction," *IEEE Transactions on Medical Imaging*, vol. 37, no. 2, pp. 491–503, 2018.
- [20] Y. Yang, J. Sun, H. Li, and Z. Xu, "Deep ADMM-Net for compressive sensing MRI," in *Advances in Neural Information Processing Systems*, 2016, pp. 10–18.
- [21] K. Hammernik, T. Klatzer, E. Kobler, M. P. Recht, D. K. Sodickson, Thomas Pock, and Florian Knoll, "Learning a variational network for reconstruction of accelerated MRI data," *Magnetic resonance in medicine*, vol. 79, no. 6, pp. 3055–3071, 2018.
- [22] Y. Romano, M. Elad, and P. Milanfar, "The Little Engine That Could: Regularization by Denoising (RED)," *SIAM Journal on Imaging Sciences*, vol. 10, no. 4, pp. 1804–1844, 2017.
- [23] G. T. Buzzard, S. H. Chan, S. Sreehari, and C. A. Bouman, "Plug-and-play unplugged: optimization-free reconstruction using consensus equilibrium," *SIAM J. Imaging Sci.*, vol. 11, no. 3, pp. 2001–20, Jan. 2018.
- [24] Y. Yang, J. Sun, H. Li, and Z. Xu, "ADMM-Net: A Deep Learning Approach for Compressive Sensing MRI," *arXiv preprint arXiv:1705.06869*, 2017.
- [25] J. Zhang and B. Ghanem, "ISTA-Net: Interpretable Optimization-Inspired Deep Network for Image Compressive Sensing," *arXiv preprint arXiv:1706.07929*, 2018.
- [26] S.U.H Dar, M. Özbey, A.B Çatlı, and T. Çukur, "A Transfer-Learning Approach for Accelerated MRI using Deep Neural Networks," *arXiv preprint arXiv:1710.02615*, 2017.
- [27] V. Antun, F. Renna, C. Poon, B. Adcock, and A. C. Hansen., "On instabilities of deep learning in image reconstruction and the potential costs of ai," *Proceedings of the National Academy of Sciences*, vol. 117, no. 48, pp. 30088–30095, May 2020.
- [28] C. Chen, Y. Liu, P. Schniter, M. Tong, K. Zareba, O. Simonetti, L. Potter, and R. Ahmad, "Ocmr (v1.0)–open-access multi-coil k-space dataset for cardiovascular magnetic resonance imaging," *arXiv preprint arXiv:2008.03410*, 2020.
- [29] J. Zbontar et al, "fastMRI: An Open Dataset and Benchmarks for Accelerated MRI," 2019, arXiv preprint arXiv:1811.08839.
- [30] K. Lei, M. Mardani, J. M. Pauly, and S. Vasanawala, "Wasserstein gans for mr imaging: From paired to unpaired training," *IEEE Transactions on Medical Imaging*, vol. 40, no. 1, pp. 105–115, Jan 2021.
- [31] T. M. Quan, T. Nguyen-Duc, and W. Jeong, "Compressed sensing MRI reconstruction using a generative adversarial network with a cyclic loss," *IEEE Transactions on Medical Imaging*, vol. 37, no. 6, pp. 1488–1497, 2018.
- [32] B. Sim, G. Oh, S. Lim, and J. C. Ye, "Optimal transport, cyclegan, and penalized ls for unsupervised learning in inverse problems," *arXiv preprint arXiv:1909.12116*, 2019.
- [33] D. Ulyanov, A. Vedaldi, and V. Lempitsky, "Deep image prior," in *Proceedings of the IEEE Conference on Computer Vision and Pattern Recognition*, 2018, pp. 9446–9454.
- [34] M. Z. Darestani and R. Heckel, "Accelerated MRI with un-trained neural networks," *arXiv preprint arXiv:2007.02471*, 2021.
- [35] B. Yaman, S. A. H. Hosseini, S. Moeller, J. Ellermann, K. Ugurbil, and M. Akcakay, "Self-supervised learning of physics-guided reconstruction neural networks without fully sampled reference data," *Magnetic Resonance in Medicine*, vol. 84, no. 6, pp. 3172–3191, 2020.
- [36] A. Lahiri, S. Ravishankar, and J. A. Fessler, "Combining supervised and semi-blind dictionary (Super-BReD) learning for MRI reconstruction," in *Proc. Intl. Soc. Mag. Res. Med.*, 2020, p. 3456.
- [37] S. Liang, A. Sreevatsa, A. Lahiri, and S. Ravishankar, "LONDn-MRI: Adaptive Local Neighborhood-Based Networks for MR Image Reconstruction from Undersampled Data," in *2022 IEEE 19th International Symposium on Biomedical Imaging (ISBI)*, 2022, pp. 1–4.
- [38] M. Lustig, D. Donoho, and J. M. Pauly, "Sparse MRI: The application of compressed sensing for rapid MR imaging," *Mag. Res. Med.*, vol. 58, no. 6, pp. 1182–95, Dec. 2007.
- [39] C. Crockett and J. A. Fessler, "Bilevel methods for image reconstruction," *arXiv preprint arXiv:2109.09610*, 2021.
- [40] F. Knoll et al, "fastMRI: A Publicly Available Raw k-Space and DICOM Dataset of Knee Images for Accelerated MR Image Reconstruction Using Machine Learning," *Radiology: Artificial Intelligence*, vol. 2, no. 1, pp. e190007, 2020.
- [41] M. Uecker, "mrirecon/bart: version 0.4.03," Apr. 2018.
- [42] Z. Wang, A.C. Bovik, H.R. Sheikh, and P.E. Simoncelli, "Image quality assessment: From error visibility to structural similarity," *IEEE Trans. Image Process.*, vol. 13, no. 4, pp. 600–612, 2004.
- [43] S. Yu, B. Park, and J. Jeong, "Deep iterative down-up cnn for image denoising," in *2019 IEEE/CVF Conference on Computer Vision and Pattern Recognition Workshops (CVPRW)*, 2019, pp. 2095–2103.
- [44] A. Lahiri, G. Wang, S. Ravishankar, and J.A. Fessler, "Blind Primed Supervised (BLIPS) Learning for MR Image Reconstruction," *IEEE Transactions on Medical Imaging*, vol. 40, no. 11, pp. 3113–3124, 2021.
- [45] M. Kaya and H. Ş. bilge, "Deep metric learning: A survey," *Symmetry*, vol. 11, no. 9, 2019.